# Potential Difference Measurements of Ocular Surface $Na^+$ Absorption Analyzed Using an Electrokinetic Model

*Marc H. Levin,*[1,2] *Jung Kyung Kim,*[1,3] *Jie Hu,*[1,3] *and A. S. Verkman*[1,2]

**Purpose.** Corneal and conjunctival epithelia are capable of transcellular $Na^+$ absorption and $Cl^-$ secretion, which drives water movement across these tissues. A recent study demonstrated with a new open-circuit potential difference (PD) technique that $Cl^-$ moves across the ocular surface in mice through $Ca^{2+}$- and cAMP-sensitive $Cl^-$ channels, the latter pathway being the cystic fibrosis (CF) transmembrane conductance regulator (CFTR). The purpose of the present study was to identify transporting mechanisms involved in $Na^+$ absorption and to develop a mathematical model of ocular surface ion transport to quantify the relative magnitudes of and electrochemical coupling among transporting processes.

**Methods.** PDs across the fluid-bathed ocular surface were measured in anesthetized wild-type and CF mice in response to $Na^+$, $Cl^-$, and $K^+$ ion substitution and transporter agonists, inhibitors, and substrates. An electrokinetic model of the ocular surface epithelium was developed to simulate PD measurements, which involved computation of membrane potentials and cell [$Na^+$], [$K^+$], [$Cl^-$] and volume from transporter activities and extracellular ion concentrations.

**Results.** $Na^+$ replacement produced a 6 ± 2-mV depolarization that was blocked by amiloride ($K_i$ 0.8 $\mu$M) and benzamil ($K_i$ 0.2 $\mu$M). The $Na^+$-dependent depolarization by amiloride was significantly greater in CF mice (19 ± 3 mV). In wild-type mice, D-, but not L-glucose produced a phloridzin-sensitive, 4.1-mV hyperpolarization in the presence of $Na^+$ and amiloride, with a $K_m$ for D-glucose of 2.5 mM. Glycine and L-arginine also produced $Na^+$-dependent hyperpolarizations. The epithelial transport model accurately reproduced experimental PD measurements.

**Conclusions.** PD measurements coupled with model computations defined quantitatively the roles of $Na^+$ and $Cl^-$ transport processes in ocular surface ion and fluid secretion, and indicated that CFTR-dependent changes in apparent epithelial $Na^+$ channel (ENaC) activity could be accounted for by electrochemical coupling, without requiring ENaC-CFTR interactions. The data and modeling also predicted significant enhancement of ocular surface fluid secretion by ENaC inhibitors and CFTR activators as possible therapies for dry eye syndromes. (*Invest Ophthalmol Vis Sci.* 2006;47:306–316) DOI:10.1167/iovs.05-1082

The ocular surface, lined by corneal and conjunctival epithelia, can actively absorb $Na^+$ from and secrete $Cl^-$ into the tear film (reviewed by Dartt[1] and Candia[2]). The relative magnitudes of net $Na^+$ absorption and $Cl^-$ secretion largely dictate the direction and magnitude of fluid movement across the ocular surface. A quantitative, mechanistic understanding of ocular surface ion transport is important in understanding the pathophysiology of dry eye conditions, or keratoconjunctivitis sicca (KCS), and in identifying targets for development of therapies to treat KCS. At present, INS365, a uridine triphosphate (UTP) agonist that stimulates chloride-fluid secretion through as yet unidentified channels, is in phase III clinical trials for treatment of KCS.[3] The purpose of this study was to establish, through experimental electrical potential measurements and mathematical modeling, a quantitative description of ion transport at the ocular surface.

We recently introduced an open-circuit potential difference (PD) method to study ion transport at the ocular surface in vivo.[4] In this method, electrical potentials generated at the superfused ocular surface (with respect to the body) are measured by a high-impedance voltmeter in response to ion substitution, agonist-inhibitor addition, or other maneuvers. Surface PDs arise from polarized ion conductances in apical and basolateral membranes across tight epithelia and so can provide, in principle, quantitative information about electrogenic transporting systems. The corneal and conjunctival surfaces are superfused as a single compartment in this method to mimic native tear film physiology, allowing assessment of the relative contributions of individual transporters to tear film homeostasis. In our initial study, CFTR was identified as a major route for $Cl^-$ secretion across the ocular surface into the tear film, and CFTR activators were proposed as a possible therapy for dry eye conditions.

In the current study, we extend the initial experimental analysis of ocular surface $Cl^-$ transport to include $Na^+$-transporting mechanisms and, by mathematical modeling, to assess the contributions of individual ion transporting pathways to net solute and fluid movement across the ocular surface. Prior experimental data with regard to $Na^+$ channels include short-circuit current experiments on in vitro albino rabbit cornea and conjunctiva, where amiloride-sensitive $Na^+$ conductance could not be demonstrated.[5,6] However, short-circuit measurements on excised bovine cornea,[7] and more recently on primary cultures of rabbit corneal epithelium,[8] have provided functional evidence for amiloride-sensitive channels. Of potential relevance to human ocular disorders, the epithelial $Na^+$ channel (ENaC) subunit proteins have been localized to the apical membrane of human corneal epithelium.[9]

In this study, ocular surface PDs were used to identify and characterize $Na^+$ channel and $Na^+$-coupled glucose- and amino acid-transporting pathways at ocular surface epithelia in living mice. A model of ocular surface epithelial ion transport was

From the [1]Departments of Medicine and Physiology and the Cardiovascular Research Institute, and the [2]Graduate Group in Biophysics, University of California, San Francisco, California.

[3]Contributed equally to the work and therefore should be considered equivalent authors.

Supported by Grants EY13574 from the National Eye Institute; DK72517 and DK35124 from the National Institute of Diabetes and Digestive and Kidney Diseases; HL73856 and HL59198 from the National Heart, Lung, and Blood Institute; EB00415 from the National Institutes of Biomedical Imaging and Bioengineering; and Drug Discovery and Research Development Program grants from the Cystic Fibrosis Foundation.

Submitted for publication August 16, 2005; revised September 19, 2005; accepted November 22, 2005.

Disclosure: **M.H. Levin**, None; **J.K. Kim**, None; **J. Hu**, None; **A.S. Verkman**, None

The publication costs of this article were defrayed in part by page charge payment. This article must therefore be marked "*advertisement*" in accordance with 18 U.S.C. §1734 solely to indicate this fact.

Corresponding author: Alan S. Verkman, 1246 Health Sciences East Tower, Cardiovascular Research Institute, University of California, San Francisco, San Francisco, CA 94143-0521; verkman@itsa.ucsf.edu.

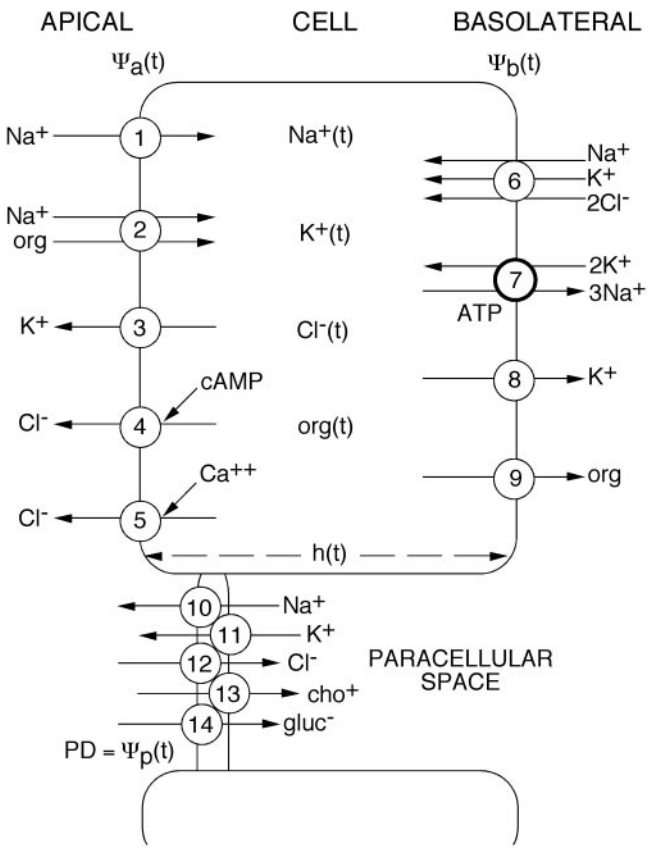


**FIGURE 1.** Ocular surface epithelial cell ion transport. Transport pathways are numbered and time-dependent intracellular solute activities, cell height, and membrane potentials are shown. Solute fluxes are defined as positive in the *left* (apical) to *right* (basolateral) direction. *Arrowheads*: direction of solute movement under open-circuit conditions. See Table A2 for specific transporter parameters under baseline, steady state conditions.

developed to compare quantitatively the rates of $Na^+$ absorption versus $Cl^-$ secretion and to analyze mechanisms of proposed coupling between CFTR and ENaC.[10,11] Modeling computations were applied to test the hypotheses that ENaC provides a quantitatively significant mechanism for ocular surface fluid transport that may be exploited for therapy of KCS and that enhanced $Na^+$ absorption in CF mice can be accounted for by CFTR-ENaC electrochemical coupling. The mathematical model describing ocular surface epithelial transport is an extension of prior models developed by our laboratory and others for non-ocular epithelial ion transport.[12–14] Figure 1 diagrams the transporting systems and pathways included in the model. The model allowed the computation of epithelial cell membrane potentials and currents, transepithelial water flow, and cellular [$Na^+$], [$K^+$], [$Cl^-$] and volume in response to experimental maneuvers such as transporter activation-inhibition and ion substitution. Although such an epithelial transport model contains multiple parameters, constraints imposed by experimental observations allowed little freedom in selecting model parameters. The model was able to reproduce experimental findings closely and to provide quantitative information and insights not otherwise possible.

## METHODS

### Mice

Wild-type and CF mice (homozygous ΔF508 mutant mice)[15] on a CD1 genetic background were bred and cared for at the University of California, San Francisco, Animal Facility. Wild-type mice were fed a standard diet, and CF mice were fed a nutritional supplement (Peptamen; Nestlé, Vevey, Switzerland). Mice aged 8 to 12 weeks weighing 25 to 30 g were used. Protocols were approved by the University of California, San Francisco, Committee on Animal Research and were in compliance with the ARVO Statement for the Use of Animals in Ophthalmic and Vision Research.

Mice were anesthetized with 125 mg/kg 2,2,2-tribromoethanol (Avertin; Sigma-Aldrich, St. Louis, MO) intraperitoneally, with supplementation during experiments to maintain deep anesthesia. Mice were immobilized, with the eye under study oriented to face upward in a custom-built stereotaxic device equipped with a rotating jaw clamp. Corneas were kept hydrated with isosmolar saline (PBS with NaCl added to give 320 mOsM) before measurements began. Core temperature was monitored with a rectal probe and maintained at 37 ± 1°C with a heating pad.

### Measurement of Ocular Surface PD

PD was measured continuously, with the ocular surface perfused serially with different solutions, as described in detail previously.[4] Briefly, solutions were perfused at 6 mL/min through plastic tubing using a multireservoir gravity pinch-valve system (ALA Scientific, Westbury, NY) and a variable-flow peristaltic pump (medium flow model; Fisher Scientific, Fair Lawn, NJ). An ~50-μL fluid reservoir was maintained at the ocular surface by surface tension, with the probe catheter (PE-90 polyethylene tubing) fixed ~1 mm from the eye surface by a micropositioner and a suction cannula positioned ~3 mm from the orbit. Solution exchange time was generally less than 3 seconds. The measuring and reference electrodes consisted of Ag/AgCl with 1-M KCl agar bridges. The measuring electrode was located near the catheter probe and connected to a high-impedance digital voltmeter (IsoMillivolt Meter; World Precision Instruments, Sarasota, FL), having input and system electrical resistances of $10^{12}$ and $1.1 \times 10^6$ Ω, respectively. The reference electrode was connected via a continuous liquid (320 mOsM saline) column to a winged, 21-gauge needle inserted in the subcutaneous tissue at the back of the neck. PDs were recorded at 5 Hz with a 14-bit analog-to-digital converter.

### Solutions and Compounds

All perfusion solutions were isosmolar to mouse serum (320 ± 5 mOsM) as measured by freezing point-depression osmometry (Precision Systems, Inc., Natick, MA). Solution compositions are listed in Table 1. Solution 1 (control solution) was PBS supplemented with 30 mOsM NaCl. Solution 2 ($Na^+$-free solution) was made by replacing NaCl with choline chloride and $Na_2HPO_4$ with 8 mM phosphoric acid, titrating to pH 7.4 with choline base and then adding choline chloride to achieve 320 mOsM. In some experiments, NaCl was replaced isosmotically with 30 mM D-glucose, L-glucose, or D-mannitol (solution 3). In solution 4, choline chloride (from solution 3) was replaced isosmotically with 30 mM D-glucose or D-mannitol. Solutions 1 and 3 or 2 and 4 were mixed to give solutions of intermediate organic solute concentrations. In solution 5 (low $Cl^-$ solution; 4.7 mM $Cl^-$), most $Cl^-$ was replaced by gluconate. Solution 6 (high-$K^+$ solution; 174.2 mM $K^+$) differed from solution 1 in that NaCl and $Na_2HPO_4$ were replaced by equimolar amounts of KCl and $K_2HPO_4$. Whereas $Cl^-$ replacement produced a small junction potential (generally ~ +1 mV) that was measured daily and used to correct PDs measured with low-$Cl^-$ perfusates, $Na^+$-free and high-$K^+$ solutions did not produce junction potentials.

Compounds were purchased from Sigma-Aldrich unless indicated otherwise. Inhibitors, activators, and substrates used in the perfusates included amiloride or benzamil (0.1–100 μM), phloridzin (100 μM), forskolin (10 μM), and L-arginine or glycine (0.1–10 mM, freshly dissolved in perfusate). $CFTR_{inh}$-172 (3-[(3-trifluoromethyl)phenyl]-5-(3-carboxyphenyl) methylene]-2-thioxo-4-thiazolidinone; 10 μM) was synthesized as described.[16] In protocols in which solution 5 (low-$Cl^-$ solution) was used, all solutions contained 10 μM indomethacin to

**TABLE 1.** Composition of Perfusate Solutions

| Solution | Name | $Na^+$ | $Cl^-$ | $K^+$ | Gluconate$^-$ | Choline$^+$ | Organic |
|---|---|---|---|---|---|---|---|
| 1 | Control | 170 | 160 | 4.2 | 0 | 0 | 0 |
| 2 | $Na^+$-free | 0 | 160 | 4.2 | 0 | 170 | 0 |
| 3 | Organic | 154 | 144 | 4.2 | 0 | 0 | 30 |
| 4 | Organic ($-Na^+$) | 0 | 144 | 4.2 | 0 | 154 | 30 |
| 5 | Low $Cl^-$ | 170 | 4.7 | 4.2 | 155 | 0 | 0 |
| 6 | High $K^+$ | 0 | 160 | 174.2 | 0 | 0 | 0 |

Values are expressed in millimolar. All solutions contained (in mM): 9.5 phosphate, 1 $Ca^{2+}$, 0.5 $Mg^{2+}$ (pH 7.40). Organic is D-glucose, L-glucose, or D-mannitol.

suppress CFTR activation by mechanical or other stimulation under control (unstimulated) conditions, as discussed previously.[4] Inhibitors-activators were prepared as 1000× stock solutions in dimethyl sulfoxide (DMSO), unless otherwise indicated.

## PD Protocols and Data Analysis

$Na^+$ transport was studied by measuring PDs during continuous perfusion of the ocular surface with a series of solutions that imposed $Na^+$ gradients and contained transporter substrates and/or inhibitors. $Cl^-$ channel function was assessed with protocols described previously.[4] Data are expressed as the mean ± SE of absolute PDs or changes in PD (ΔPD), and statistical comparisons between groups were made with the two-tailed Student's *t*-test.

## Model Formulation

**Overview.** The model treats the ocular surface as an infinite, homogeneous monolayer of cells containing transcellular and paracellular solute transport pathways (Fig. 1). Programming was done using Visual Fortran (Compaq; Hewlett Packard, Palo Alto, CA). Intracellular solute activities, cell membrane potentials, and cell height (reflecting volume) were allowed to vary in time. Mucosal and serosal compartments consisted of infinite well-stirred solute pools with compositions that could be altered at specified time(s). Transporting systems for $Na^+$, $K^+$, and $Cl^-$ were included in the model.

In ocular surface epithelia, the basolateral ouabain-sensitive $3Na^+/2K^+$ATPase (transporter 7) establishes the electrochemical potential that drives electroneutral (bumetanide-inhibitable) $Na^+/K^+/2Cl^-$ symport (transporter 6). $Na^+$ can also enter cells through an amiloride-sensitive $Na^+$ channel (transporter 1), and organic solute-coupled cotransporters (transporter 2). Distinct glucose- and amino-acid transporters, assumed to be coupled 1:1 to $Na^+$ based on data from rabbit conjunctiva[17,18] are represented in the model as a single "$Na^+$-org" transporter. A neutral exit pathway for organic solutes is included that represents cellular efflux and/or utilization (transporter 9). $Cl^-$ secretion occurs at the apical membrane through transporter 4, now known to be the cAMP-regulated $Cl^-$ channel CFTR, as well as a $Ca^{2+}$-activated Cl channel (transporter 5). Apical and basolateral $K^+$ conductances are included as possible exit pathways for $K^+$ (transporters 3 and 8). Paracellular pathways for all charged species (transporters 10–14) are also included. Although cellular pH regulation may be important in cornea and conjunctiva, bicarbonate and proton transport pathways are not considered significant determinants of ocular surface fluid transport, as seen by the small, ~2-mV bicarbonate effect on ocular PD.[4] As such, bicarbonate transport and $Na^+/H^+$ exchange pathways are not included in this model.

**Parameters.** Definitions and units of symbols are listed in Table 2. Transporter permeability coefficients were determined from open-circuit ion flux and membrane potential data (see Tables A1 and A2 in the Appendix) deduced from measured ocular PDs and literature values, as explained in the Appendix. Solute activities were related to absolute concentrations and osmotic activities according to intracellular and extracellular activity and osmotic coefficients, as listed in Table A3.

Solute flux ($J_i^X$) through each membrane and paracellular transport pathway was defined as a function of solute concentrations on each side of the membrane and, if electrogenic, a membrane potential. Electrodiffusive flux of solute $X$ through the $i$th transport pathway was assumed to be nonsaturable and nonallosteric, unless otherwise noted, as given by the Goldman-Hodgkin-Katz equation:

$$J_i^X = P_i z_i U_z (X_1 - X_2 e^{-z_i U_z})/(1 - e^{-z_i U_z}), \quad (1)$$

where $P_i$ is the permeability coefficient (in centimeters per second), $z_i$ is the ionic charge, and $X_1$ and $X_2$ are the activities of transported solute (in millimolar) in compartments to the left and right of the diffusive barrier, respectively. $U_z$, the dimensionless membrane potential, is related to the appropriate potential difference ($\psi_z$) in Table 2. Equations for flux through each transport pathway ($J_i^X$), and the resultant net apical, basolateral, and paracellular currents ($I_a$, $I_b$, and $I_p$) are provided in the Appendix (equations A1–A17).

**Numerical Solution.** Cell membrane potentials at time ($t + \Delta t$) were calculated iteratively with the Newton-Raphson method based on electroneutral conditions. The open-circuit model requires equal opposing transcellular and paracellular currents ($I_a = I_b = -I_p$). An option was included to model transport under short-circuit conditions, where $I_a = I_b$ and $U_a = U_b$. $U_a$ and $U_b$ were computed iteratively by

**TABLE 2.** Model Symbols and Definitions

| | |
|---|---|
| $X(t)$ | Activity of solute $X$ in cytoplasm (mM) |
| $X_a$ | Activity of solute $X$ in apical bathing solution (mM) |
| $X_b$ | Activity of solute $X$ in basolateral bathing solution (mM) |
| $a_x$ | Cellular activity coefficient of solute $X$ |
| $\phi_x$ | Cellular osmotic coefficient of solute $X$ |
| $a_x^e$ | Extracellular activity coefficient of solute $X$ |
| $\phi_x^e$ | Extracellular osmotic coefficient of solute $X$ |
| $\psi_s$ | Serum osmolarity (units vary and are specified for each equation) |
| $h(t)$ | Cell height (μm) |
| $J_i$ | Turnover rate of $i$th transporter (Fig. 1). Solute flux for $X$ is the product of $J_i$ and the number of $X$ transported per turnover event ($J_i^x$, μeq/cm$^2$ per second), defined as positive from left to right |
| $I_a$ | Apical-to-cell membrane current (μA/cm$^2$) |
| $I_b$ | Cell-to-basolateral membrane current (μA/cm$^2$) |
| $I_p$ | Apical-to-basolateral paracellular current (μA/cm$^2$) |
| $P_i$ | Permeability coefficient for $i$th transporter (units provided in Table A2) |
| $K_i^x$ | Apparent binding constant for solute $X$ to transporter $i$ (mM), used for saturable transporters as described in the Appendix. |
| $\psi_a$ | Apical membrane potential (cell with respect to apical solution); (mV) |
| $\psi_b$ | Basolateral membrane potential (cell with respect to basolateral solution); (mV) |
| $\psi_t$ | Transepithelial potential (PD; $\psi_b - \psi_a$); (mV) |
| $U_z$ | Dimensionless potential ($U_z = \psi_z F/RT$, where F = 23 cal/mV per mole, $R$ = 1.9872 cal/K per mole, and $T$ = 310 K) |

user-supplied initial guess. Assuming instantaneous osmotic equilibration and constant cell surface area, cell height $h(t + \Delta t)$ (in micrometers) was computed as

$$h(t + \Delta t) = h(t) + \Delta t \Sigma^{a-b} \phi_x J_i^X / \psi_s. \quad (2)$$

$\Sigma^{a-b} \phi_x J_i^X$ generically represents the net osmotic flux (in milliosmolar per square centimeter per second) into the cell and is related to individual transporter fluxes in equation A18. $\psi_s$ is mouse serum osmolarity (in milliOsmols per cubic centimeter). Intracellular solute activities were computed from fluxes and the updated cell height from equation 2 according to

$$X(t + \Delta t) = [X(t)h(t) + \Delta t \Sigma a_x J_i^X]/h(t + \Delta t). \quad (3)$$

$\Sigma a_x J_i^X$ is defined as the net rate of entry of active solute $X$ (in $10^4$ meq/cm$^2$ per second) into the cellular compartment through the various transporters. Refer to equations A19–A22 for the specific expressions used in computing $Na^+(t + \Delta t)$, $K^+(t + \Delta t)$, $Cl^-(t + \Delta t)$, and $org(t + \Delta t)$. The model also offers the option to impose brief current or voltage spikes (one each minute) to compute total tissue resistance. The observed change in voltage or current can be used to monitor transepithelial electrical resistance (TEER, in kilo-ohms per square centimeter) under open- or short-circuit conditions, respectively (TEER = $\Delta\psi_t/\Delta I_a$). Though the exact mechanism of transepithelial fluid movement remains controversial, it is agreed that it results in near-isosmolar water flux driven by solute transport. As such, net transepithelial water secretion or absorption (microliters per square centimeter per hour) was computed assuming isosmolar fluid flow across the apical membrane and paracellular tight-junctional barrier by

$$J_v(t + \Delta t) = \Sigma^{a+p} \phi_x J_i^X / \psi_s, \quad (4)$$

where $\Sigma^{a+p} \phi_x J_i^X$ is the net osmotic flux (in milliOsmols per square centimeter per second) into the apical compartment from individual transport pathway fluxes (equation A23), and $\psi_s$ is serum osmolarity (in Osmols per liter).

## Results

### Amiloride-Sensitive $Na^+$ Transport

$Na^+$ channel function was studied by using ion replacement and transporter substrates and inhibitors. Baseline PD was first established (using solution 1) before replacement of perfusate $Na^+$ by the relatively impermeant cation choline (solution 2). This exchange produced a 5- to 10-mV depolarization that was reversed by reintroduction of $Na^+$ (solution 1). Representative PD recordings in Figure 2A show the reversible changes in PD on $Na^+$ substitution, depolarization by amiloride (100 $\mu$M) in the presence of a $Na^+$-containing perfusate (left), and blocking of the $Na^+$-induced hyperpolarization by amiloride (right). Dose-inhibition studies were performed for amiloride and its analogue, benzamil. A representative dose–response curve for amiloride is shown in Figure 2B (left). $K_i$ was 0.82 $\mu$M for amiloride and 0.22 $\mu$M for benzamil (right). These data indicate the involvement of amiloride- and benzamil-sensitive $Na^+$ channel(s) in ocular surface $Na^+$ absorption, which is probably ENaC.

To determine the contribution of the other major cation $K^+$ to apical electrogenic transport, experiments were performed using a high-$K^+$ solution (solution 6). Amiloride was first added to solution 1 to minimize the influence of $Na^+$ channel function on interpretation of PDs in terms of $K^+$ channel function. Switching to solution 6 produced a very small 1- to 2-mV reversible hyperpolarization (data not shown, $n = 5$ separate experiments). Model computations supported the conclusion

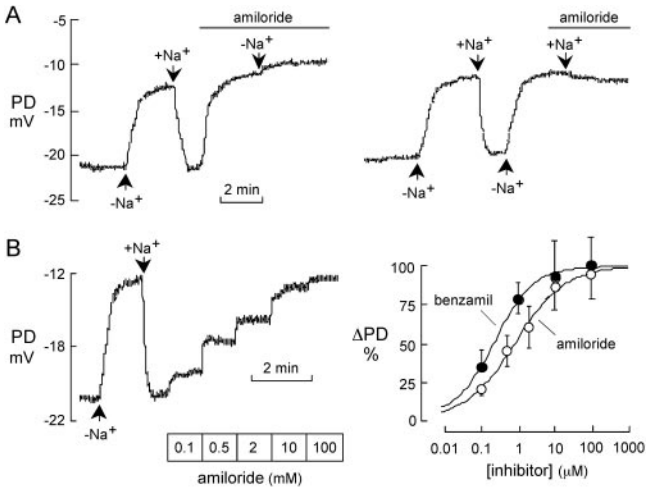


**Figure 2.** Amiloride-sensitive $Na^+$ transport at the ocular surface. (**A**) PD recordings showing effects of switching between sodium-containing ($+Na^+$) and sodium-free ($-Na^+$, sodium replaced by choline) solutions. *Horizontal line*: presence of amiloride, added to either the $+Na^+$ (*left*) or $-Na^+$ (*right*) solutions. Representative of six experiments. Solutions used were *left*: 1 alone, 2 alone, 1 alone, 1+amiloride, and 2+amiloride; *right*: 1 alone, 2 alone, 1 alone, 2 alone, and 2+amiloride. (**B**) Dose-dependent inhibition of sodium absorption by amiloride and benzamil. *Left*: Representative time course of PD inhibition, first by $Na^+$ replacement, and then by adding amiloride to the perfusate at increasing concentrations. Solutions used: 1 alone, 2 alone, 1 alone, and 1+amiloride. *Right*: dose response of benzamil and amiloride for depolarizing PD, determined from experiments as shown on the *left* (mean ± SE, $n = 5$ for benzamil; $n = 6$ for amiloride).

that apical $K^+$ conductance is much lower than apical $Na^+$ or $Cl^-$ conductance.

**Ion Transport in CF Mice.** Ocular surface $Cl^-$ transport was assayed as described previously.[4] Figure 3A shows PD data from wild-type versus CF mice in which baseline PDs (of similar values) were first recorded with solution 1. Switching to an amiloride-containing solution depolarized ocular surface PDs, with CF mice showing a significantly greater response (15–20 mV in CF vs. 5–10 mV in wild-type mice). Replacing most $Cl^-$ by the relatively impermeant anion gluconate (solution 5) gave a sustained hyperpolarization in wild-type but not CF mice, which is related to cAMP- but not CFTR-independent $Cl^-$ secretion. The CFTR agonist forskolin produced a further hyperpolarization in wild-type mice that was reversed by $CFTR_{inh}$-172.

The protocol used in Figure 2A was applied to investigate amiloride-sensitive $Na^+$ conductance in CF mice. Representative PD recordings in Figure 3B (left) show reversible depolarizations in wild-type and CF mice in response to $Na^+$ substitution. Depolarizations of similar magnitude were produced by amiloride (100 $\mu$M) in the presence of $Na^+$-containing perfusate. The CF mice consistently showed greater responses than wild-type mice to both $Na^+$ replacement and amiloride addition. As summarized in Figure 3B (right), $Na^+$ replacement and amiloride administration produced ΔPDs of 20 ± 3 and 19 ± 2 mV, (SE, $n = 6$) in CF mice, respectively. The same maneuvers produced 6 ± 2- and 7 ± 1-mV depolarizations in wild-type mice ($n = 6$). These results indicate the presence of an amiloride-sensitive $Na^+$ channel at the ocular surface, with apparent increased activity in CF mice.

**Modeling Ocular Surface $Na^+$ and $Cl^-$ Transport.** The PD measurements suggest that active $Na^+$ and $Cl^-$ transport processes dictate net fluid movement across corneal-conjunctival epithelia, and comparative experiments performed on wild-type versus CF mice suggest a complex interaction among

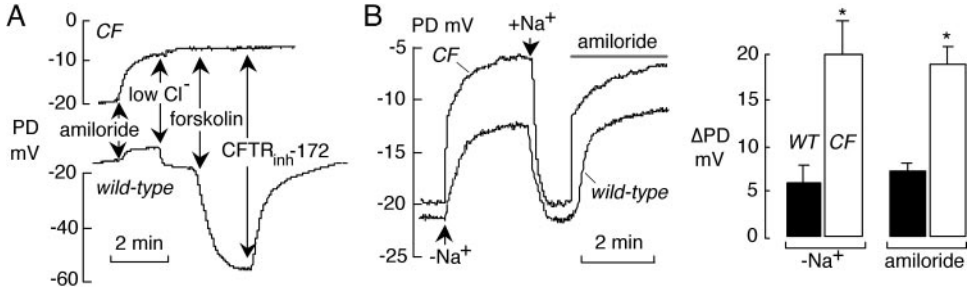


**FIGURE 3.** Ion transport at the ocular surface in CF mice. (**A**) PD recordings in CF (*top*) and wild-type (*bottom*) mice in response to amiloride, low $Cl^-$, forskolin (10 $\mu$M), and $CFTR_{inh}$-172 (10 $\mu$M). Solutions used: 1 alone, 1+amiloride, 5+amiloride, 5+amiloride+forskolin, and 5+amiloride+forskolin+$CFTR_{inh}$-172. (**B**) Elevated amiloride-sensitive $Na^+$ absorption in CF mice. *Left*: PD tracings in wild-type versus CF mice (curves overlaid) in response to $Na^+$ replacement and amiloride. Solutions used: 1 alone, 2 alone, 1 alone, and 1+amiloride. *Right*: Summary of $\Delta$PD for wild-type and CF mice for indicated maneuvers (SE, $n = 6$ eyes per genotype). $^*P <$ 0.01 comparing wild-type versus CF mice.

these pathways. As such, we developed a model to gain better qualitative understanding and to define quantitatively the key determinants of active ocular surface fluid secretion.

According to the model in Figure 1 with parameters for the ocular surface of wild-type mice selected as described in the Appendix, Figure 4A shows the time course of the major cellular variables in mice after "inhibition" (by amiloride) of transporter 1 (ENaC conductance). Before inhibition, all parameters were stable to within 0.01% for a 60-minute simulation (not shown). The top graph shows the time-dependent apical, basolateral, and transepithelial potentials ($\psi_a$, $\psi_b$, and PD). Conductances were chosen to give a baseline PD of $-23$ mV and a ratio of active $Na^+$ to $Cl^-$ flux of 1:1, which produced a 5.5-mV amiloride-induced PD depolarization. The second graph shows total transepithelial current before and after amiloride. The steady-state current of 8.0 $\mu A/cm^2$ was reduced by 22% by ENaC inhibition. The current spikes produced by the periodic brief voltage spikes gave a baseline TEER of 5.3 $k\Omega/cm^2$, which increased to 6.8 $k\Omega/cm^2$ after amiloride addition. The bottom two panels in Figure 4A show the influence of apical $Na^+$ conductance on the three major intracellular ions and cell height. There was a small decrease in cell height consequent to reduced cellular $Na^+$. Secondarily enhanced transport of $K^+$ into the cell produced a small 0.4% final increase in cell height. In general, each cell parameter reached a new steady state within minutes after inhibition of transporter 1.

Figure 4B shows the time-dependent PD response in open-circuit conditions after a series of maneuvers commonly used to elucidate transport mechanisms. As seen in the top graph, simulated $Na^+$ replacement by choline yielded a depolarization similar to the experimental findings in Figures 2A and 3B. The immediate and sustained hyperpolarization of 9.5 mV predicted on replacing most apical $Cl^-$ with gluconate (solution 1 switched to solution 5) also replicated experimental trends. The bottom two panels predict the time course of PD reduction toward zero after basolateral inhibition of the lone source of cellular $Cl^-$, the $Na^+/K^+/2Cl^-$ symporter (transporter 6), and the transepithelial current generator, the $3Na^+/2K^+$ATPase (transporter 7). Because the electroneutral $Na^+/K^+/2Cl^-$ symporter lacks a membrane-potential dependence, no immediate change in PD was present on its inhibition.

The main findings from ocular PD experiments were modeled. In Figure 5A, the protocol for studying chloride transport was simulated, with initial ENaC inhibition, followed serially by switching to a low-$Cl^-$ solution, addition of a CFTR activator, and then addition of a CFTR inhibitor. This simulation resembled experimental PD data (as in Fig. 3A, top) with one exception. Simulated instantaneous $Cl^-$ channel activation yielded a significant transient hyperpolarization followed by more modest sustained hyperpolarization. Such PD behavior is not seen experimentally in response to either forskolin or direct CFTR activators, but is observed after addition of UTP.[4] Of note, incorporating rectification into the basolateral $K^+$ channel

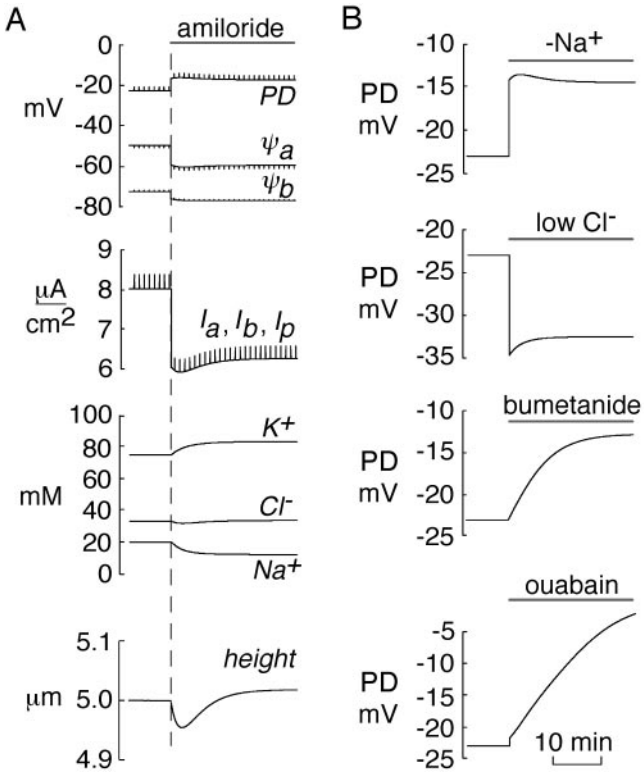


**FIGURE 4.** Ocular surface epithelial ion transport model. For each maneuver, individual transporter conductances or apical compartment solute compositions were changed instantaneously. See the Appendix for model parameters. (**A**) Influence of amiloride on time-dependent model parameters in open-circuit conditions. Transporter 1 (apical $Na^+$) conductance was fully inhibited (at *dashed line*). Changes in (from *top* to *bottom*) membrane potentials, currents, intracellular ion activities, and cell height are shown. Brief voltage spikes were applied every minute (*top tracings*) by an imposed current spike (*second trace* from *top*) with a magnitude that was a fixed proportion of the instantaneous current. (**B**) Effects of different maneuvers on open-circuit PD. From top to bottom, apical $Na^+$ replaced with choline, apical $Cl^-$ replaced by gluconate, basolateral $Na^+/K^+/2Cl^-$ symporter inhibited, and basolateral $3Na^+/2K^+$ ATPase inhibited.

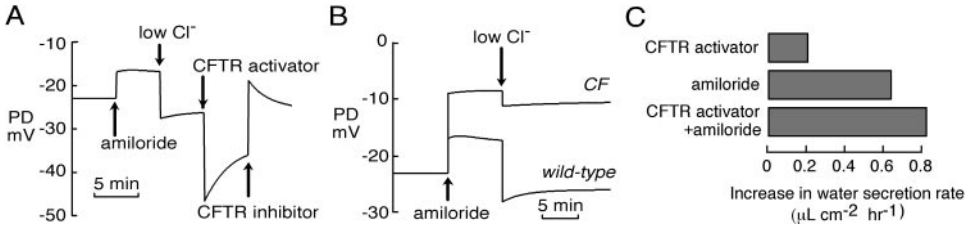


**FIGURE 5.** Modeling PD protocols and fluid secretion. (**A**) Simulation of protocol for studying chloride transport (as in the experiment in Fig. 3A). CFTR activation was produced by a threefold increase in apical $Cl^-$ permeability. (**B**) Simulation of protocol for studying sodium transport. Comparison of wild-type versus CF mouse ocular PDs in response to amiloride and then low $Cl^-$. Solutions simulated: 1 alone, 1+amiloride, and 5+amiloride. CF mouse apical $Cl^-$ permeability was 20% of that in wild-type mouse, whereas apical $Na^+$ permeability was not changed in the CF mouse parameter set. (**C**) Incremental steady state water secretion (above baseline), modeled in response to addition to solution 1 of amiloride, a CFTR activator (increasing apical $Cl^-$ conductance threefold), or both together.

(transporter 8) conductance (as described by Horsiberger[11]) did not alter this general behavior. To mimic the finite solution exchange time and the noninstantaneous time course of CFTR activation after addition of the agonist, an additional simulation was performed in which apical chloride conductance was increased to the same extent, but over 4 minutes (not shown). The slower channel activation blunted much of the transient hyperpolarization, but did not change steady state PD.

Direct CFTR activators and the general cAMP agonist forskolin have been found to elicit nearly identical diffusion potentials under low-$Cl^-$ conditions.[4] To test whether isolated CFTR activation can be predicted to enhance apical $Cl^-$ secretion in a manner similar to forskolin, simulations were performed in which basolateral $K^+$ (transporter 8) conductance was activated to various degrees along with CFTR. Indeed, only a small augmentation of CFTR-activator–induced hyperpolarization could be achieved by concurrent stimulation of basolateral $K^+$ conductance (−35.4-mV PD after threefold CFTR and $K^+$ channel activation vs. −34.4 mV for CFTR activation alone, not shown). These findings have implications regarding strategies of pharmacological modulation of fluid secretion (see the Discussion section).

The simulation in Figure 5B focused on the difference in amiloride effect in wild-type versus CF mice (as seen in Figs. 3A, 3B) and the possibility of CFTR-ENaC interactions. Model parameters for wild-type and CF mice were chosen to yield identical baseline PDs of −23 mV, as reported previously[4] and depicted in Figure 3B. Apical $Cl^-$ permeability in CF mice was chosen to be 20% of that in wild-type mice, to recapitulate the observed amiloride effect in CF mice whereas $Na^+$ conductance was fixed to that in wild-type mice. As seen in Figure 5B, PD depolarized by 14.5 mV upon ENaC inhibition in CF mice, similar to that measured in Figure 3B. Switching the apical compartment to a low-$Cl^-$ solution (solution 5) correctly predicted a small diffusion potential of 2.1 mV in CF mice, compared with the 8.7-mV hyperpolarization in wild-type mice. Simulations were also performed in which ENaC permeability was increased twofold (using parameters from CF or wild-type mice), examining effects of ENaC inhibition and low-$Cl^-$ substitution. ENaC inhibition yielded depolarizations of 19 and 10 mV with CF and wild-type parameters, respectively, and hyperpolarizations of 4.1 and 8.8 mV for low $Cl^-$. In both cases, ENaC hyperactivity produced substantial low-$Cl^-$ effects, which was inconsistent with experimental findings. Of importance, the model reproduced the major ocular surface electrophysiological properties in wild-type and CF mice only in the absence of CFTR-dependent ENaC conductance (see the Discussion section).

By assuming isosmolar fluid secretion, implying fixed coupling between transepithelial solute and water transport, we also modeled the ability of transporter modulators to increase transepithelial water secretion. Computations were performed under physiological conditions (in the absence of transepithelial ionic gradients) to simulate compound action on fluid secretion into the native tear film. Figure 5C shows that both ENaC inhibition and CFTR activation increased net fluid secretion by inhibiting $Na^+$ absorption and enhancing $Cl^-$ secretion, respectively, and that the effects were additive.

**Organic Solute-Coupled $Na^+$ Transport.** In addition to amiloride-sensitive $Na^+$ channels, electrogenic $Na^+$ transport across the ocular surface, and thus fluid secretion, may also involve $Na^+$-glucose and $Na^+$-amino acid cotransport. Figure 6A (left) shows that isosmolar addition of D-glucose but not of D-mannitol produced a small hyperpolarization that was reversed by the $Na^+$-glucose cotransporter inhibitor phloridzin. L-Glucose (5 mM) produced no significant change in PD (data not shown, $n = 4$ eyes). Under physiological conditions of high apical $Na^+$ concentration, extracellular D-glucose saturability ($K_m$) was 2.5 mM as measured from PDs at increasing concentrations of D-glucose (Fig. 6A, middle and right). Hill analysis gave a D-glucose-$Na^+$ coupling ratio of 0.89, consistent with 1:1 $Na^+$-glucose cotransport. The PD data in Figure 6A were modeled to determine the turnover rates of transporters 2 and 9 (see Appendix for explanation of parameter selection). Modeling of the experimentally measured ~4-mV hyperpolarization under conditions of saturated cotransport and tonic ENaC inhibition (Fig. 6B) indicated a $J_2$ (SGLT-1) turnover equal to ~75% of the $J_1$ (ENaC) basal activity (0.11 vs. 0.15 $\mu$eq/cm$^2$ per hour). Because SGLT-1 likely transports two solutes per turnover, this implies similar osmolar absorptive capacities of amiloride-insensitive and amiloride-sensitive pathways.

The basic and neutral amino acids L-arginine and glycine also produced small, reversible hyperpolarizations in the presence of $Na^+$ (Fig. 6C). Amino acid transport was saturated only at relatively high concentration (several mM) for both amino acids studied. L-Arginine and glycine, added at 10 mM, yielded hyperpolarizations of 1.5 ± 0.9 mV ($n = 4$, SE) and 2.1 ± 0.4 mV ($n = 5$), respectively. PD analysis also revealed competitive substrate binding, where addition of L-arginine to glycine-containing solution reproducibly caused a depolarization (Fig. 6C, right). The $Na^+$ dependence of these electrogenic pathways of glucose and amino acid absorption was confirmed. Figure 6D (left) shows hyperpolarizations produced by 5 mM D-glucose and 1 mM L-arginine (but not mannitol) in the presence of $Na^+$ and amiloride. The hyperpolarizations were abolished after $Na^+$ replacement by choline. Averaged results are summarized in Figure 6D (right). Together, these results provide evidence for at least three distinct electrogenic $Na^+$ pathways at the ocular surface: amiloride-sensitive $Na^+$ channels, $Na^+$-glucose cotransport, and $Na^+$-amino acid cotransport.

## DISCUSSION

The goals of this study were to identify experimentally and to quantify by modeling the major $Na^+$-transporting pathways at the ocular surface and to use experimental and modeling results to examine the roles of epithelial transporters in driving

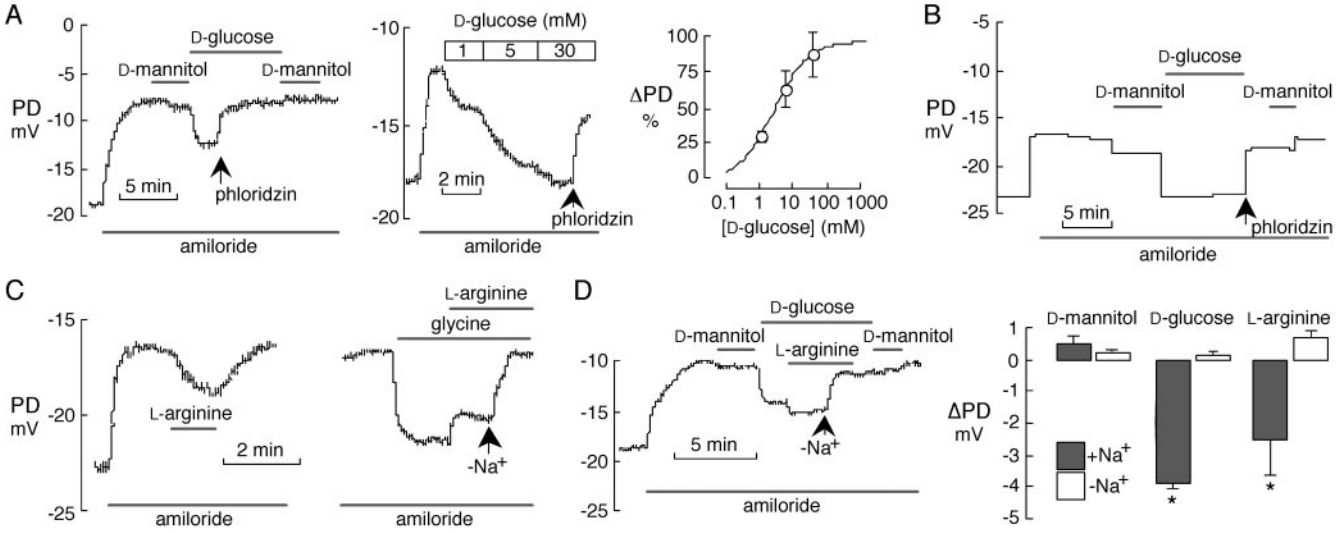


**FIGURE 6.** Solute-coupled $Na^+$ absorption. (**A**) *Left*: PD response to additions of D-mannitol (30 mOsM, replacing NaCl) and D-glucose (30 mOsM, replacing D-mannitol), followed by the $Na^+$-glucose cotransporter inhibitor phloridzin (100 $\mu$M), all in solutions containing amiloride (100 $\mu$M). Solutions used: 1 alone, 1+amiloride, 3(D-mannitol)+ amiloride, 3(D-glucose)+amiloride, 3(D-glucose)+amiloride+phloridzin, 3(D-mannitol)+amiloride+phloridzin, and 1+amiloride+phloridzin. *Middle*: Concentration-dependent effect of D-glucose on PD in the presence of amiloride (100 $\mu$M). Solutions used: 1 alone, 1+amiloride, and a series of mixtures of 1 and 3(D-glucose)+amiloride. *Right*: Corresponding concentration–response curve (mean ± SE, $n = 5$). (**B**) Simulated PD tracing of maneuvers identical with those performed experimentally and depicted in (**A**, *left*). (**C**) PD responses to amino acids, in the presence of amiloride. *Left*: L-arginine (1 mM) was added to and then removed from solution 1. Representative of six experiments. Solutions used: 1 alone, 1+amiloride, 1+amiloride+L-arginine, and 1+amiloride. *Right*: addition to solution 1 of glycine (5 mM) followed by L-arginine (5 mM) before $Na^+$ replacement by choline. Representative of four experiments. Solutions used: 1+amiloride, 1+amiloride+glycine, 1+amiloride+glycine+L-arginine, and 2+amiloride+glycine+L-arginine. (**D**) *Left*: representative PD response to serial isosmolar additions of 30 mM D-mannitol, 30 mM D-glucose, and 1 mM L-arginine in the presence of amiloride. Solutions used: 1 alone, 1+amiloride, 3(D-mannitol)+amiloride, 3(D-glucose)+amiloride, 3(D-glucose)+amiloride+L-arginine, 4(D-glucose)+amiloride+L-arginine, 4(D-glucose)+amiloride, 4(D-mannitol)+amiloride, and 2+amiloride. *Right*: Paired analysis of ΔPD measured in $+Na^+$ or $-Na^+$ solutions. SE, $n = 3$–5 mice; $^*P < 0.01$, comparing PD responses to zero.

fluid secretion and putative CFTR-ENaC interactions. This approach provides a framework to define electrochemical coupling relevant to a variety of epithelial disorders, and for ocular surface epithelium, this approach allowed us to predict computationally the efficacy of therapies for states of tear deficiency. The PD measurement method is technically simple and permits minimally invasive in vivo measurements under physiological open-circuit conditions. The high-resistance epithelial surface, comprising cornea and conjunctiva in parallel, is responsible for generating and maintaining a large PD. The dependence of ocular PDs on specific $Na^+$ and $Cl^-$ transport processes, combined with transport agonist-inhibitor and ion substitution maneuvers, allows for rapid qualitative assessment of solute transport in vivo. In this study, we extended the PD measurement concept by developing a mathematical model to rigorously relate measured PDs to transporter permeabilities and transporting mechanisms.

A major role for amiloride-sensitive apical $Na^+$ absorption was found, which, according to the model, was equal in magnitude to total net $Cl^-$ secretion. The inhibitory half-concentrations of amiloride ($K_i$, 0.82 mM) and benzamil ($K_i$, 0.22 mM) measured are in close agreement with those reported recently in primary cultures of pigmented rabbit corneal epithelial cells[8] and are consistent with the greater potency of benzamil than amiloride for ENaC. Comparable depolarizations were observed for $Na^+$ replacement and amiloride application in both wild-type and CF mice, suggesting that amiloride-sensitive $Na^+$ conductance provides the primary route for apical membrane $Na^+$ transport under the experimental conditions (solution 1, which lacks D-glucose and amino acids). Modeling of fluid secretion in the absence of an ionic gradient predicted that $Na^+$ channel inhibition or CFTR $Cl^-$ channel activation would increase fluid secretion into the tear film and that both together would provide an even greater benefit than either strategy alone.

In contrast to the large measured apical $Na^+$ conductance, a weak dependence of ocular surface PD on perfusate $K^+$ concentration was found in the presence of amiloride, indicating a relatively small apical surface $K^+$ conductance. Similar results were reported for human nasal epithelia.[19] At steady state, basolateral $K^+$ channels enhance the electrochemical driving force for fluid secretion. However, modeling of PDs in this study predicted that increased basolateral $K^+$ conductance would augment apical $Cl^-$ secretion little, suggesting that CFTR-specific activators would be as effective as general cAMP agonists (which activate CFTR and some basolateral $K^+$ channels) in increasing apical chloride-driven fluid secretion.

Ocular surface PD measurements also provided direct evidence for transepithelial glucose- and amino acid-coupled $Na^+$ absorption. The kinetics of substrate activation for the $Na^+$-glucose cotransporter (SGLT-1) varies widely among species.[20] Whereas tear $Na^+$ concentration (>100 mM) is thought to provide a saturating concentration for $Na^+$ ($K_m \sim 60$ mM), the affinity of SGLT-1 for glucose must be determined experimentally for a given system. The $K_m$ of 2.5 mM for glucose measured in this study is lower than that of 16.7 mM measured in rabbit conjunctiva.[18] The relatively low concentration of glucose in the normal human tear film (~200 $\mu$M) is unlikely to cause significant fluid absorption.[20] However, elevated tear glucose may contribute to the ocular surface disease noted in hyperglycemic diabetes (~1 mM) by producing net absorption in the steady state.[21,22] This prediction is supported by data in rabbits obtained by Shiue et al.,[23] who found a ~75% reduction in transconjunctival fluid secretion upon apical addition of saturating glucose.

$Na^+$-dependent neutral–basic amino acid cotransport has also been characterized in rabbit conjunctiva, where both high (micromolar $K_m$)- and low (millimolar $K_m$)-affinity processes have been described for L-arginine.[17] We measured qualitatively significant absorption at superphysiologic (in millimolar) amino acid concentrations, compared with the low-micromolar values reported by Puck et al.[24] in native tear film. Thus, although $Na^+$-coupled amino acid cotransport may not be relevant to steady-state tear fluid balance, our results support the strategy of delivering ocular therapeutics, either as amino acid analogues or conjugates, through cotransporters.[25]

Although both corneal and conjunctiva epithelia are complex multilayered tissues, the ocular surface epithelial cell is modeled in the current study as a single cell layer with a parallel shunt, as was done previously to study passive solute fluxes across corneal epithelium.[26] Measurements in rabbit corneal epithelium have documented intimate electrical connection among superficial and wing cell layers, in support of this assumption.[27] Moreover, the apical superficial cell membrane largely dictates the electrical properties of stratified ocular surface epithelia because of its highly resistive tight junctions.[27,28] The magnitudes of flux chosen in this simulation yielded a TEER of 5.3 $k\Omega/cm^2$, between the range of 12 to 17 $k\Omega/cm^2$ measured under short-circuit conditions in rabbit cornea[5,29] and that of 1 to 2 $k\Omega/cm^2$ reported in rabbit conjunctiva.[6,17,25] A potential weakness of the current model is the simplistic consideration of paracellular conductances in the context of a complicated multilayered epithelium, where possible unstirred layers could affect intercellular solute movement. In polarized epithelia that can both absorb and secrete ions to comparable extents, such as those lining the ocular surface, relative paracellular ion conductances largely determine the degree of basal fluid absorption and secretion.[29] However, the treatment of paracellular conductance would only affect estimates of basal fluid secretion and not predictions regarding the utility of membrane-transport modulators. Relative impermeant-to-permeant paracellular ion permeabilities of 0.7 were selected for anions and cations, to reproduce the minimal effect of $Na^+$ replacement by choline or $K^+$ in the presence of amiloride. Of note, these parameters are also in accord with the measurements of Amasheh et al.[30]

As has been found in nasal PD measurements in CF versus wild-type mice[31,32] and CF versus non-CF human subjects,[19] amiloride produced a much greater depolarization at the ocular surface in CF versus wild-type mice (seen in Fig. 3). We also found an enhanced depolarization in CF mice after $Na^+$ replacement. There is ongoing controversy regarding the mechanism responsible for these apparent CFTR-ENaC interactions. Whereas some studies have suggested direct inhibition of ENaC function by CFTR,[10,33] recent modeling and careful experimentation suggest that electrochemical coupling accounts for the apparent hyperabsorption of $Na^+$ across CF epithelia.[11,34] We investigated purported CFTR-ENaC interactions by modeling the system with parameters for CF mice chosen to test whether enhanced $Na^+$ absorption across CF epithelia can be explained by electrochemical coupling between parallel-functioning transporters. PDs from the CF mouse ocular surface were accurately simulated with fivefold reduced apical $Cl^-$ conductance, yet identical $Na^+$ conductance, compared with wild-type mice, indicating that direct regulation of ENaC by CFTR by a mechanism other than electrochemical coupling is not necessary to explain the experimental results. Although CF epithelia are predicted to have 20% of normal function, both experiments and modeling suggest that most of the unstimulated (cAMP- and $Ca^{2+}$-independent) $Cl^-$ flux passes through CFTR-dependent channels, though not through CFTR itself. We showed previously that the low-$Cl^-$ hyperpolarization in wild-type mice was reversed only to a small extent by a CFTR inhibitor.[4] Our model also demonstrated that reduced apical $Cl^-$ conductance and unaltered $Na^+$ absorptive capacity were both necessary to abolish most of the low $Cl^-$ effect in CF mice (2.1-mV hyperpolarization predicted in CF as found experimentally).

In conclusion, our results define quantitatively the principal $Na^+$-transporting pathways at the ocular surface and the electrochemical coupling between $Na^+$ and $Cl^-$ transport in wild-type and CF ocular surface epithelia. The model predicted significant enhancement of serosal-to-mucosal fluid transport by $Na^+$ channel inhibitors and $Cl^-$ channel activators. Direct measurement of fluid secretion across the intact ocular surface and studies in animal models of dry eye syndrome are needed to guide and validate the modeling of fluid secretion.

### *Acknowledgments*

The authors thank Liman Qian for mouse breeding and genotype analysis and Oscar Candia for advice on model parameter selection.

## APPENDIX

### Model Flux Equations

For electrogenic fluxes, individual transport pathways were governed by simple electrodiffusion unless otherwise specified, with fluxes defined by the Goldman-Hodgkin-Katz equation (equation 1 in the main text). Neutral transport pathways lacked a potential dependence. Each equation is provided below, along with any necessary explanation.

$$J_1 = P_1 U_a [Na_a^+ - Na^+(t) e^{-U_a}]/(1 - e^{-U_a}). \quad (A1)$$

$$J_2 = P_2 U_a \frac{Na_a^+ org_a - Na^+(t) org(t) e^{-U_a}}{\left(\frac{Na_a^+}{K_2^{Na}} + 1\right)\left(\frac{org_a}{K_2^{org}} + 1\right)(1 - e^{-U_a})}. \quad (A2)$$

Transporter 2, when modeled as the $Na^+$-glucose cotransporter, was assigned extracellular saturability values for both $Na^+$ ($K_2^{Na}$) and glucose ($K_2^{org}$). $K_2^{Na}$ was assumed to be 60 mM based on data of Horibe et al.[18] in rabbit conjunctiva. $K_2^{org}$ was determined experimentally to be 2.5 mM at the mouse ocular surface by dose–response experiments under conditions of saturating apical $Na^+$.

$$J_3 = P_3 U_a [K_a^+ - K^+(t) e^{-U_a}]/(1 - e^{-U_a}), \quad (A3)$$

$$J_4 = -P_4 U_a [Cl_a^- - Cl^-(t) e^{U_a}]/(1 - e^{U_a}), \quad (A4)$$

$$J_5 = -P_5 U_a [Cl_a^- - Cl^-(t) e^{U_a}]/(1 - e^{U_a}), \quad (A5)$$

$$J_6 = P_6 \frac{Na^+(t) K^+(t) Cl^-(t)^2 - Na_b^+ K_b^- (Cl_b^-)^2}{\left[1 + \frac{Na_b^+}{K_6^{Na}}\right]\left[1 + \frac{K_b^+}{K_6^K}\right]\left[1 + \frac{Cl_b^-}{K_6^{Cl}}\right]^2}, \quad (A6)$$

$$J_7 = P_7 \left[\frac{Na^+(t)}{Na^+(t) + K_7^{Na}}\right]^3 \left[\frac{K^+(t)}{K_b^+ + K_7^K}\right]^2 (a \cdot U_b + b). \quad (A7)$$

Flux equations for transporters 6 and 7 (the $Na^+/K^+/2Cl^-$ symporter and $3Na^+/2K^+$ATPase) were identical with those used in the model of tracheal epithelia by Hartmann and Verkman.[14] Saturability (in millimolar) was assigned accordingly ($K_6^{Na} = 3.8$; $K_6^K = 7.5$; $K_6^{Cl} = 26$; $K_7^{Na} = 11.8$; and $K_7^K = 1.4$), as were the constants in equation A7 that define the weak

**TABLE A1.** Baseline, Steady State Cell Parameters for Wild-Type Mouse Open-Circuit PDs

| | Apical | Cell | Basolateral |
|---|---|---|---|
| Solute activities (mM) | | | |
| $Na^+$ | 119 | 20 | 112 |
| $Cl^-$ | 112 | 33 | 84 |
| $K^+$ | 3.3 | 75 | 3.2 |
| Organic* | 30 | 20 | 10 |
| Net active ion flux ($\mu$eq/cm$^2$ per hour) | | $J_{Na^+}$ 0.15 | $J_{Cl^-}$ −0.15 |
| Membrane potential (mV) | $\psi_a$ −50 | $\psi_b$ −73 | $\psi_p$ −23 |

* Organic (D-glucose) was absent from most apical perfusates but was included at 30 mM when calculating $P_2$ and $P_9$.

basolateral membrane potential dependence of $3Na^+/2K^+$ATPase ($a = 0.006$; $b = 1 - a \cdot U_b$).

$$J_8 = P_8 U_b [K^+(t) - K_b^+ e^{-U_b}]/(1 - e^{-U_b}), \quad (A8)$$

$$J_9 = P_9 [org(t) - org_b], \quad (A9)$$

$$J_{10} = P_{10} U_p [Na_a^+ - Na_b^+ e^{-U_p}]/(1 - e^{-U_p}), \quad (A10)$$

$$J_{11} = P_{11} U_p [K_a^+ - K_b^+ e^{-U_p}]/(1 - e^{-U_p}), \quad (A11)$$

$$J_{12} = -P_{12} U_p [Cl_a^- - Cl_b^- e^{U_p}]/(1 - e^{U_p}), \quad (A12)$$

$$J_{13} = P_{13} U_p [chol_a^+ - chol_b^+ e^{-U_p}]/(1 - e^{-U_p}), \quad (A13)$$

$$J_{14} = -P_{14} U_p [gluc_a^- - gluc_b^- e^{U_p}]/(1 - e^{U_p}) \quad (A14)$$

## Model Parameter Selection

Transporter permeability coefficients were calculated from the flux equations using estimated ion activities, membrane potentials, and net transcellular $Na^+$ and $Cl^-$ fluxes under open-circuit conditions (see Table A1 for a summary of parameters for simulations in wild-type mice). Apical ion activities were chosen from the composition of solution 1. Basolateral ion activities were assigned based on serum concentrations from CD1 wild-type mice (measured by the University of California, San Francisco, Moffitt Hospital Clinical Laboratory; $n = 5$). Cellular ion activities and apical and basolateral membrane potentials were estimated from intracellular microelectrode measurements made in frog and rabbit corneal epithelial in vitro systems.[35,36] Baseline cellular $Cl^-$ activity was set at 33 mM, 1.9-fold greater than predicted for passive distribution across the apical membrane.[35] Values of −50 and −73 mV were chosen for $\psi_a$ and $\psi_b$, respectively, to yield the experimentally measured steady state transepithelial potential ($\psi_a - \psi_b = -23$ mV).

All transcellular permeability coefficients (with the exceptions of $P_2$ and $P_9$) were determined from estimated steady state net active $Na^+$ and $Cl^-$ fluxes. The ratio of active $Na^+$ absorption to $Cl^-$ secretion (1:1 in wild-type mice and 5:1 in CF mice) was deduced experimentally from the magnitude of the amiloride effect, as described in the Results and Discussion sections. Because no levels of ion fluxes across mouse ocular surface epithelia have been determined, the absolute magnitudes of active $Na^+$ and $Cl^-$ flux for wild-type mice were chosen as intermediate values between those for cornea and conjunctiva, which were reported from rabbit and frog under both open- and short-circuit conditions.[6,8,17,18,29]

We had some freedom in selecting the relative apical and basolateral $K^+$ fluxes ($J_3$ and $J_8$, respectively). However, modeling of the very weak experimentally determined dependence of PD on apical $K^+$ confirmed that most of the $K^+$ flux occurred through transporter 8 ($J_3$: $J_8 = -1$:224 in wild-type mice). Paracellular permeability values were selected based on the small effect of $Na^+$ replacement on PD (see Fig. 2A). Equal and opposing transcellular and paracellular $Na^+$ fluxes were assumed.[29] A combination of higher assumed baseline absolute transcellular $Na^+$ and $Cl^-$ and relative paracellular $Na^+$ flux values would increase the predicted baseline ocular surface fluid secretion rate. Based on constraints imposed by our own experimental observations and in accordance with flux measurements through tight junctions,[30] $Na^+$ and $K^+$ permeabilities ($P_{10}$ and $P_{11}$) were assumed to be equal, with relative selectivity for choline$^+$ versus $Na^+$ and $K^+$ as $P_{13}$: $P_{10}$: $P_{11}$ = 0.7:1:1, and for gluconate versus chloride as $P_{14}$: $P_{12}$ = 0.7:1 (Table A2).

Simulations involving $Na^+$-organic cotransport (Fig. 6B) focused on $Na^+$-coupled glucose permeation. $P_2$ was chosen to produce in simulations the 4- to 5-mV hyperpolarization measured experimentally in the presence of amiloride. $P_9$ was then selected to give equal apical and basolateral membrane glucose fluxes in the steady state ($J_2 = J_9$). Parameters for these

**TABLE A2.** Transporter Permeabilities and Baseline, Steady-State Fluxes

| Transporter | $P_i$ | Units | $J_i$ ($\mu$eq/cm$^2$, per hour) |
|---|---|---|---|
| Apical membrane | | | |
| 1 $Na^+$ conductance | $1.63 \times 10^{-7}$ | cm/s | 0.15 |
| 2 $Na^+$/org symporter | $1.43 \times 10^{-7}$ | cm/s · mM$^{-2}$ | 0.11 |
| 3 $K^+$ conductance | $1.52 \times 10^{-8}$ | cm/s | −0.001 |
| 4/5 $Cl^-$ conductance | $1.21 \times 10^{-6}$ | cm/s | −0.15 |
| Basolateral membrane | | | |
| 6 $Na^+/K^+/2Cl^-$ symporter | $1.81 \times 10^{-8}$ | cm/s · mM$^{-4}$ | 0.075 |
| 7 $3Na^+/2K^+$ ATPase | $1.73 \times 10^{-4}$ | $\mu$mol · cm$^{-2}$ · s | 0.075 |
| 8 $K^+$ conductance | $1.24 \times 10^{-5}$ | cm/s | 0.224 |
| 9 Org conductance | $3.06 \times 10^{-6}$ | cm/s | 0.11 |
| Paracellular | | | |
| 10 $Na^+$ conductance | $4.54 \times 10^{-7}$ | cm/s | −0.15 |
| 11 $K^+$ conductance | $4.54 \times 10^{-7}$ | cm/s | −0.00439 |
| 12 $Cl^-$ conductance | $3.53 \times 10^{-7}$ | cm/s | 0.145 |
| 13 Choline$^+$ conductance | $3.18 \times 10^{-7}$ | cm/s | — |
| 14 Gluconate$^-$ conductance | $2.47 \times 10^{-7}$ | cm/s | — |

Transporter numbers correspond to those depicted in Figure 1.

**TABLE A3.** Activity and Osmotic Coefficients

| Solute | $a_x$ | $\phi_x$ | $a_x^e$ | $\phi_x^e$ |
|---|---|---|---|---|
| $Na^+$, $K^+$, $Cl^-$ | 0.75 | 0.7 | 0.75 | 0.92 |
| org | 1 | 1 | 1 | 1 |

simulations were selected based on the intracellular $Na^+$ activity (12.1 mM) and $\psi_a$ (−59.9 mV) achieved after amiloride addition and on the apical $Na^+$ and $Cl^-$ contents of solution 3.

## Iterative Procedure

Computations in this study were performed under open-circuit conditions. Fluxes through each transport conduit were computed using the guesses for $\psi_a$ and $\psi_b$ over time intervals of $\Delta t = 1$ second. Computations using a smaller step size ($\Delta t =$ 0.1 second) gave similar results, confirming the adequacy of the 1-second step size. Total currents across each major barrier were then calculated at the end of each time interval:

$$I_a = 96500 \cdot (J_1 + J_2 + J_3 - J_4 - J_5), \quad (A15)$$

$$I_b = 96500 \cdot (J_7 + J_8), \quad (A16)$$

$$I_p = 96500 \cdot (J_{10} + J_{11} - J_{12} + J_{13} - J_{14}), \quad (A17)$$

where 96,500 represents Faraday's constant, which converts flux into current. The threshold for acceptable relative deviation from open-circuit electroneutrality was set at 0.01%. If boundary conditions were not met, both $\psi_a$ and $\psi_b$ were modified by 1 mV and the two-dimensional Newton-Raphson method was used to update guesses for both $\psi_a$ and $\psi_b$ for the next iteration.

Once electroneutrality was established ($I_a = I_b = -I_p$), changes in cell volume (expressed as height, assuming a constant surface area) were computed based on net isosmolar water fluxes. The equation for computing net osmotically active solute flux into the cellular compartment is

$$\Sigma^{a-b}\phi_X J_i^X = \phi_{Na}J_1 + (\phi_{Na} + \phi_{org})J_2 + \phi_K J_3 + \phi_{Cl}J_4 + \phi_{Cl}J_5 - (\phi_{Na} + \phi_K + 2\phi_{Cl})J_6 - (3\phi_{Na} - 2\phi_K)J_7 - \phi_K J_8 - \phi_{org}J_9. \quad (A18)$$

Steady state cell height was assumed to be 5 $\mu$m, similar to the height of the superficial ocular surface cell layer. The exact choice of cell height was important only for pre–steady-state kinetics after perturbation. Employing the updated cell height as well as solute fluxes, new intracellular solute activities at time ($t + \Delta t$) were computed:

$$Na^+(t + \Delta t) = [Na^+(t) \cdot h(t) + \Delta t \cdot a_{Na} \cdot 10^4 \cdot (J_1 + J_2 - J_6 - 3J_7)]/h(t + \Delta t), \quad (A19)$$

$$K^+(t + \Delta t) = [K^+(t) \cdot h(t) + \Delta t \cdot a_K \cdot 10^4 \cdot (J_3 + 2J_7 - J_6 - J_8)]/h(t + \Delta t), \quad (A20)$$

$$Cl^-(t + \Delta t) = [Cl^-(t) \cdot h(t) + \Delta t \cdot a_{Cl} \cdot 10^4 \cdot (J_4 + J_5 - 2J_6)]/h(t + \Delta t), \quad (A21)$$

$$org(t + \Delta t) = [org(t) \cdot h(t) + \Delta t \cdot a_{org} \cdot 10^4 \cdot (J_2 - J_9)]/h(t + \Delta t). \quad (A22)$$

Net isosmolar water movement across the apical cell membrane and intercellular space into the apical compartment was calculated (equation 4 in the Methods section; Table A3) using the summed osmotically active solute movement:

$$\Sigma^{a+p}\phi_X J_i^X = -[\phi_{Na,e}J_1 + (\phi_{Na,e} + \phi_{org,e})J_2 + \phi_{K,e}J_3 + \phi_{Cl,e}J_4 + \phi_{Cl,e}J_5 + \phi_{Na,e}J_{10} + \phi_{K,e}J_{11} + \phi_{Cl,e}J_{12} + \phi_{cho,e}J_{13} + \phi_{gluc,e}J_{14}]. \quad (A23)$$

## *References*


1. Dartt DA. Regulation of mucin and fluid secretion by conjunctival epithelial cells. *Prog Retin Eye Res*. 2002;21:555–576.
2. Candia OA. Electrolyte and fluid transport across corneal, conjunctival, and lens epithelia. *Exp Eye Res*. 2004;78:527–535.
3. Li Y, Kuang K, Yerxa B, Wen Q, Rosskothen H, Fischbarg J. Rabbit conjunctival epithelium transports fluid and P2Y2(2) receptor agonists stimulate $Cl^-$ and fluid secretion. *Am J Physiol*. 2001;281: C595–C602.
4. Levin MH, Verkman AS. CFTR-regulated chloride transport at the ocular surface in living mice measured by potential differences. *Invest Ophthalmol Vis Sci*. 2005;46:1428–1434.
5. Marshall WS, Klyce SD. Cellular and paracellular pathway resistance in the "tight" Cl-secreting epithelium of rabbit cornea. *J Membr Biol*. 1983;73:275–282.
6. Shi XP, Candia OA. Active sodium and chloride transport across the isolated rabbit conjunctiva. *Curr Eye Res.* 1995;37:927–935.
7. Midelfart A. The effects of amiloride, ouabain, and osmolality on sodium transport across bovine cornea. *Pflugers Arch.* 1987;408: 243–248.
8. Chang-Lin JE, Kim KJ, Lee VH. Characterization of active ion transport across primary rabbit corneal epithelial cell layers (RCrECL) cultured at an air-interface. *Exp Eye Res*. 2005;60:827–836.
9. Mirshahi M, Nicolas C, Mirshahi S, Golestaneh N, d'Hermies F, Agarwal MK. Immunochemical analysis of the sodium channel in rodent and human eye. *Exp Eye Res*. 1999;69:21–32.
10. Schreiber R, Hopf A, Mall M, Greger R, Kunzelmann K. The first-nucleotide binding domain of the cystic-fibrosis transmembrane conductance regulator is important for inhibition of the epithelial $Na^+$ channel. *Proc Natl Acad Sci USA*. 1999;96:5310–5315.
11. Horisberger JD. ENaC-CFTR interactions: the role of electrical coupling of ion fluxes explored in an epithelial cell model. *Pflugers Arch*. 2003;445:522–528.
12. Latta R, Clausen C, Moore LC. General method for the derivation and numerical solution of epithelial transport models. *J Membr Biol*. 1984;82:67–82.
13. Verkman AS, Alpern RJ. Kinetic transport model for cellular regulation of pH and solute concentration in the renal proximal tubule. *Biophys J*. 1987;51:533–546.
14. Hartmann T, Verkman AS. Model of ion transport regulation in chloride-secreting airway epithelial cells. *Biophys J*. 1990;58:391–401.
15. Colledge WH, Abella BS, Southern KW, et al. Generation and characterization of a delta F508 cystic fibrosis mouse model. *Nat Genet*. 1995;10:445–452.
16. Ma T, Thiagarajah JR, Yang H, et al. Thiazolidinone CFTR inhibitor identified by high-throughput screening blocks cholera toxin-induced intestinal fluid secretion. *J Clin Invest*. 2002;110:1651–1658.
17. Hosoya K, Horibe Y, Kim KJ, Lee VH. $Na^+$-dependent L-arginine transport in the pigmented rabbit conjunctiva. *Exp Eye Res*. 1997; 65:547–553.
18. Horibe Y, Hosoya K, Kim KJ, Lee VH. Kinetic evidence for $Na^+$-glucose co-transport in the pigmented rabbit conjunctiva. *Curr Eye Res*. 1997;16:1050–1105.
19. Knowles M, Gatzy J, Boucher R. Relative ion permeability of normal and cystic fibrosis nasal epithelium. *J Clin Invest*. 1983;71: 1410–1417.

20. Hirayama BA, Lostao MP, Panayotova-Heiermann M, Loo DD, Turk E, Wright EM. Kinetic and specificity differences between rat, human, and rabbit $Na^+$-glucose cotransporters (SGLT-1). *Am J Physiol*. 1996;270:G919–G926.
21. Sen DK, Sarin GS. Tear glucose levels in normal people and in diabetic patients. *Br J Ophthalmol*. 1980;64:693–695.
22. Ozdemir M, Buyukbese MA, Cetinkaya A, Ozdemir G. Risk factors for ocular surface disorders in patients with diabetes mellitus. *Diabetes Res Clin Pract*. 2003;59:195–199.
23. Shiue MH, Kulkarni AA, Gukasyan HJ, Swisher JB, Kim KJ, Lee VH. Pharmacological modulation of fluid secretion in the pigmented rabbit conjunctiva. *Life Sci.* 2000;67:PL105–PL111.
24. Puck A, Liappis N, Hildenbrand G. Ion exchange column chromatographic investigation of free amino acids in tears of healthy adults. *Ophthalmic Res*. 1984;16:284–288.
25. Hosoya KI, Horibe Y, Kim KJ, Lee VH. Carrier-mediated transport of NG-nitro-L-arginine, a nitric oxide synthase inhibitor, in the pigmented rabbit conjunctiva. *J Pharmacol Exp Ther*. 1998;285:223–227.
26. Friedman MH. Mathematical modeling of transport in structured tissues: corneal epithelium. *Am J Physiol.* 1978;234:F215–F224.
27. Klyce SD, Wong RK. Site and mode of adrenaline action on chloride transport across the rabbit corneal epithelium. *J Physiol*. 1977;226:777–799.
28. Klyce SD. Electrical profiles in the corneal epithelium. *J Physiol*. 1972;226:407–429.
29. Klyce SD. Transport of Na, Cl, and water by the rabbit corneal epithelium at resting potential. *Am J Physiol*. 1975;228:1446–1452.
30. Amasheh S, Meiri N, Sitter AH, et al. Claudin-2 expression induces cation-selective channels in tight junctions of epithelial cells. *J Cell Sci*. 2002;115:4969–4976.
31. Grubb BR, Vick, RN, Boucher RC. Hyperabsorption of $Na^+$ and raised Ca(2+)-mediated $Cl^-$ secretion in nasal epithelia of CF mice. *Am J Physiol*. 1994;266:C1478–C1483.
32. Salinas DB, Pedemonte N, Muanprasat C, Finkbeiner WF, Nielson DW, Verkman AS. CFTR involvement in nasal potential differences in mice and pigs studied using a thiazolidinone CFTR inhibitor. *Am J Physiol*. 2004;287:L336–L347.
33. Mall M, Grubb BR, Harkema JR, O'Neal WK, Boucher RC. Increased airway epithelial $Na^+$ absorption produces cystic fibrosis-like lung disease in mice. *Nat Med*. 2004;10:487–493.
34. Nagel G, Barbry P, Chabot H, Brochiero E, Hartung K, Grygorczyk R. CFTR fails to inhibit the epithelial sodium channel ENaC, when expressed in Xenopus laevis oocytes. *J Physiol*. 2005;564:671–682.
35. Festen CM, Slegers JF, Van Os CH. Intracellular activities of chloride, potassium and sodium in rabbit corneal epithelium. *Biochim Biophys Acta*. 1983;732:394–404.
36. Reuss L, Reinach P, Weinman SA, Grady TP. Intracellular ion activities and Cl-transport mechanisms in bullfrog corneal epithelium. *Am J Physiol*. 1983;244:C336–C347.